Supporting Information

Profiling of a prescription drug library for potential transporter-based drug-drug interactions in the kidney

Yasuto Kido, Pär Matsson and Kathleen M. Giacomini*

Department of Bioengineering and Therapeutic Sciences, University of California San Francisco

**kathy.giacomini@ucsf.edu*

Table of contents

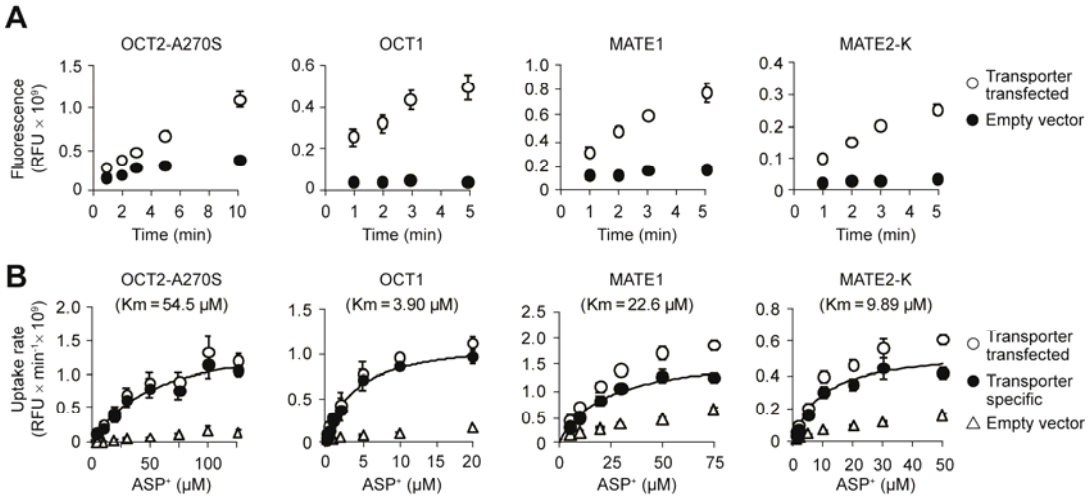

Figure S1. Development of screening assays for additional major organic cation transporters. (A) Time course of ASP^+ uptake in HEK293 cells stably expressing the OCT2-A270S genetic variant, OCT1, MATE1 and MATE2-K (open circles) and in cells transfected with an empty vector (closed circles). (B) Concentration dependence of ASP^+ uptake in transporter transfected cells (open circles) and cells transfected with an empty vector (open triangles). The transporter specific uptake (closed circles) was calculated by subtracting the non-specific uptake in empty vector transfected cells from that in the transporter transfected cells. Data are presented as mean ± s.d. (*n*=3).

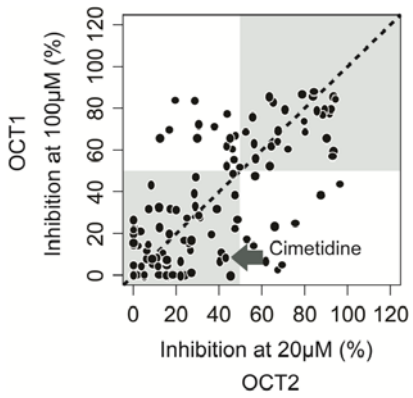

Figure S2. Comparison of inhibitor specificity between OCT2 and the hepatic paralog OCT1. Inhibition determined at 20 μM inhibitor concentration in the present study is plotted against inhibition of OCT1 determined by Ahlin, et al. (2008) at 100 μM concentration. 119 compounds were assayed in both systems. In this comparison of inhibition at five times higher concentration for OCT1 than for OCT2, 27 of the 37 OCT2 inhibitors show affinity also for OCT1.

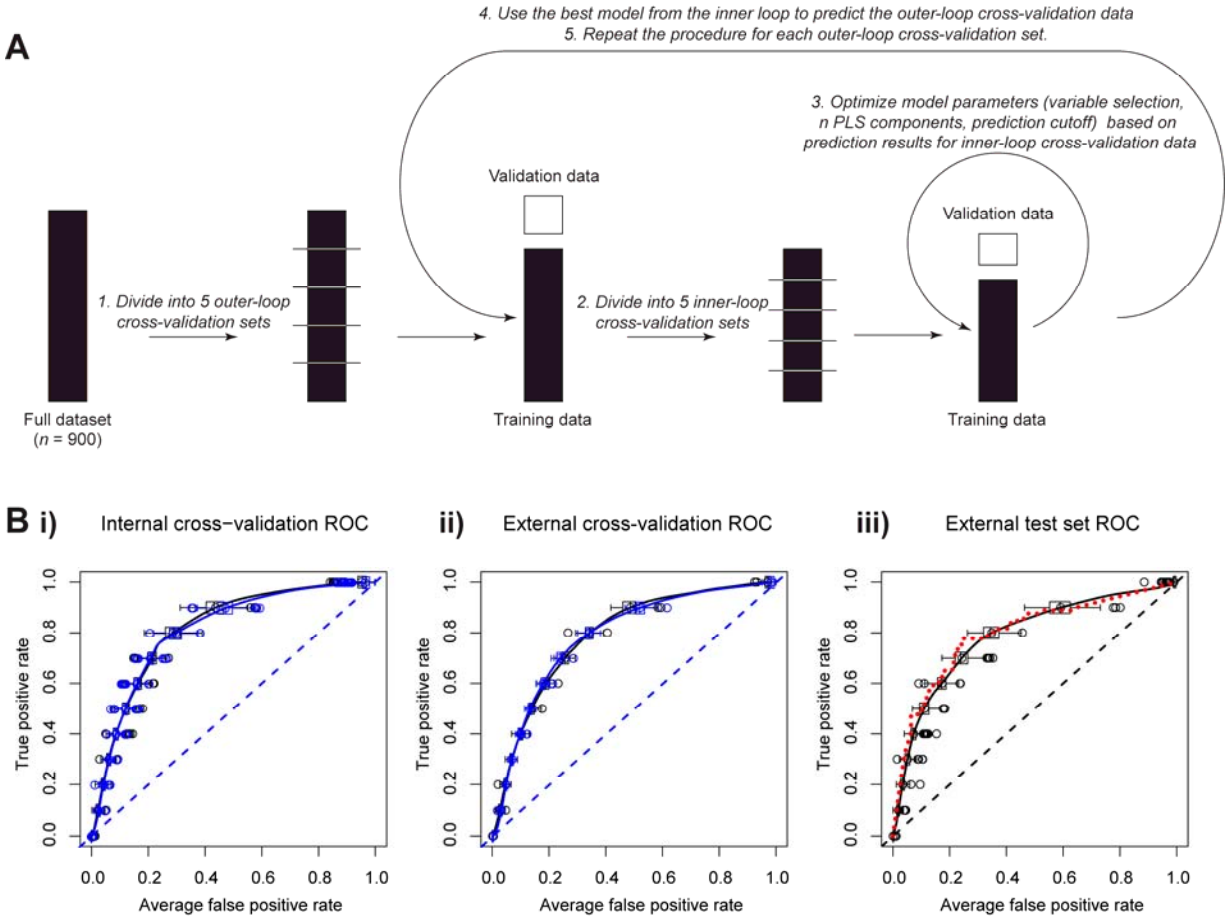

Figure S3. Development of structure-activity models.
(A) Schematic representation of the structure-activity modeling procedure. First, the dataset was randomly divided into five outer-loop CV segments. In turn, each of these segments were used as hold-out prediction sets, while the compounds in the remaining four segments were used for model training. The training data was further divided into five inner-loop cross-validation segments, and the inner loop was used to optimize model parameters and variable selection. The best model from the inner-loop optimization was then used to predict the outer-loop test set. Since all model optimization is performed in the inner loop, CV predictions in the outer loop represent an unbiased estimate of the true external model predictivity. The entire double-loop procedure was repeated 100 times for different random partitionings of the dataset to enable calculation of confidence intervals of prediction accuracy estimates and model parameters. Also, for comparison, models were developed using a random subset of the data as an external test set (*n* = 300), and using the procedure above to develop models from the remaining 600 compounds.
(B) Predictivity of models of OCT2 inhibition. Receiver operating characteristic (ROC) curves are shown for the inner-loop cross-validation (Bi), the outer-loop external cross-validation (Bii) and for an external test set (Biii). Lines and boxes show the mean and range of model predictivity estimates from all random partitionings of the data. Blue color represents statistics for models developed from the entire dataset, and black color represents statistics for models developed from a randomly selected subset of all compounds (*n* = 600), using the remaining 300 compounds as an external test set. The red dotted line represents averaged predictions of the external testset from all 500 developed models. Dashed lines illustrate the expected predictivity of a completely random model.

Table S2. Statistics for models of OCT2 inhibition.

Model set[a]	Model statistic[b]	Inner CV loop[c] Mean	Inner CV loop[c] Range	Outer CV loop[d] Mean	Outer CV loop[d] Range	External test set[e] Mean	External test set[e] Range	Consensus prediction[f]
A	n components	2.7±2.0	(1-11)					
	n variables	33.8±16.7	(11-75)					
	AUC	0.81±0.01	(0.78-0.85)	0.79±0.01	(0.74-0.81)	*n. a.*	*n. a.*	*n. a.*
	Accuracy	0.76±0.01	(0.73-0.80)	0.74±0.02	(0.68-0.79)	*n. a.*	*n. a.*	*n. a.*
	TPR Precision	0.55±0.02	(0.50-0.60)	0.51±0.02	(0.44-0.59)	*n. a.*	*n. a.*	*n. a.*
	TNR Precision	0.90±0.01	(0.88-0.91)	0.88±0.01	(0.84-0.91)	*n. a.*	*n. a.*	*n. a.*
	TPR Recall	0.76±0.01	(0.73-0.80)	0.72±0.04	(0.58-0.80)	*n. a.*	*n. a.*	*n. a.*
	TNR Recall	0.77±0.01	(0.73-0.80)	0.74±0.02	(0.67-0.82)	*n. a.*	*n. a.*	*n. a.*
	Average precision	0.72±0.01	(0.69-0.75)	0.69±0.02	(0.64-0.74)	*n. a.*	*n. a.*	*n. a.*
	Average recall	0.76±0.01	(0.73-0.80)	0.73±0.02	(0.67-0.79)	*n. a.*	*n. a.*	*n. a.*
B	n components	3.7±2.4	(1-12)					
	n variables	35.4±18.0	(9-75)					
	AUC	0.82±0.01	(0.77-0.86)	0.79±0.01	(0.77-0.81)	0.79±0.01	(0.74-0.81)	0.80
	Accuracy	0.77±0.01	(0.73-0.81)	0.73±0.01	(0.71-0.76)	0.74±0.02	(0.68-0.79)	0.75
	TPR Precision	0.55±0.02	(0.50-0.61)	0.50±0.01	(0.47-0.54)	0.51±0.02	(0.44-0.59)	0.53
	TNR Precision	0.90±0.01	(0.88-0.93)	0.87±0.01	(0.85-0.89)	0.88±0.01	(0.84-0.91)	0.89
	TPR Recall	0.76±0.02	(0.72-0.83)	0.71±0.02	(0.64-0.76)	0.72±0.04	(0.58-0.80)	0.74
	TNR Recall	0.77±0.02	(0.73-0.81)	0.74±0.02	(0.70-0.77)	0.74±0.02	(0.67-0.82)	0.76
	Average precision	0.72±0.01	(0.69-0.76)	0.69±0.01	(0.67-0.71)	0.69±0.02	(0.64-0.74)	0.71
	Average recall	0.77±0.01	(0.73-0.81)	0.72±0.01	(0.70-0.76)	0.73±0.02	(0.67-0.79)	0.75

[a] A: models developed using the entire dataset. B: models developed using a randomly selected training set (n = 600) and evaluated on the remaining compounds (n = 300).
[b] AUC: area under the receiver-operating characteristic curve; TPR: true positive rate; TNR: true negative rate.
[c] Cross-validated (CV) prediction results during the model optimization and parameter selection phase. Presented as mean ± sd for 500 models (100 random divisions for the outer loop and 5 optimized models from each inner loop).
[d] External predictions from the outer cross-validation loop. Presented as mean ± sd for 100 models (100 random divisions for the outer loop).
[e] Predictions of an external hold-out test set (n = 300). Presented as mean ± sd for all 500 models developed.
[f] Majority-vote consensus predictions of the external test set from all 500 models developed.

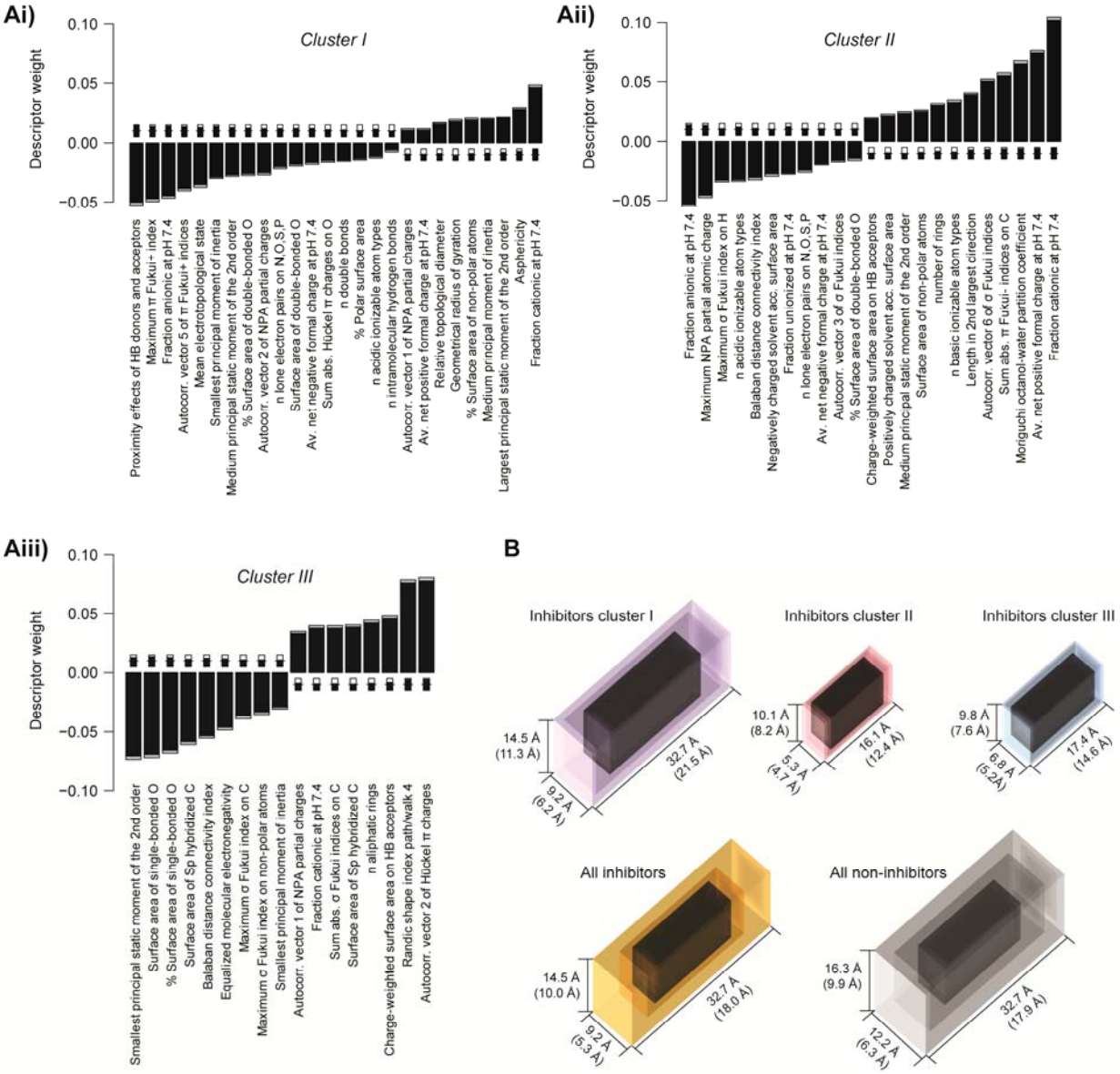

Figure S4. Molecular properties of OCT2 inhibitors in each of the three inhibitor clusters.
(A) Molecular descriptors discriminating between inhibitors and non-inhibitors in separate models for each of the three clusters. Bars show the mean PLS regression coefficients from 500 cross-validated models (100 random cross-validation partitionings with five segments each); standard errors are shown in light gray. Descriptors with positive coefficients have higher values in inhibitors, and descriptors with negative coefficients have higher values in non-inhibitors. The descriptors shown were included in at least 50% of the final 500 models after optimization through iterative exclusion of uninformative descriptors; inset thermometer plots show the fraction of all models that include the descriptor.
(B) Size distribution of inhibitors in clusters I, II, and III (top row), all inhibitors (bottom left), and all non-inhibitors (bottom right). The outermost box is the tightest enclosing one that fits all compounds in the class, and the progressively smaller boxes fit 99%, 95%, 75% and 50% of the class compounds. Dimensions are shown for the boxes that fit 100% and, in parentheses, 95% of the class.

Table S3. Assignment of reported transported OCT2 substrates in the clusters in Figure 6Av.

Compound	Cluster	Reference
Agmatine	II	Gründemann, et al., 2003
Amantadine	II	Busch, et al., 1998
ASP^+	II	Present report
Choline	II	Gorboulev, et al., 1997
Cimetidine	I	Dudley, et al., 2000
Dopamine	II	Busch, et al., 1998
Guanidine	II	Urakami, et al., 2002
Histamine	II	Busch, et al., 1998
Memantine	II	Busch, et al., 1998
N1-Methylnicotinamide	II	Gorboulev, et al., 1997
1-Methyl-4-phenylpyridinium	II	Gorboulev, et al., 1997
Norepinephrine	II	Busch, et al., 1998
Propranolol	II	Dudley, et al., 2000
Prostaglandin E2	III	Kimura, et al., 2002
Prostaglandin F2α	III	Kimura, et al., 2002
Quinine	II	Gorboulev, et al., 1997
Serotonin	II	Busch, et al., 1998
Tetraethylammonium	II	Gorboulev, et al., 1997

Supplemental References

Busch, A.E., Karbach, U., Miska, D., Gorboulev, V., Akhoundova, A., Volk, C., Arndt, P., Ulzheimer, J.C., Sonders, M.S., Baumann, C., et al. (1998). Human neurons express the polyspecific cation transporter hOCT2, which translocates monoamine neurotransmitters, amantadine, and memantine. Mol Pharmacol 54, 342-352.

Dudley, A.J., Bleasby, K., and Brown, C.D. (2000). The organic cation transporter OCT2 mediates the uptake of beta-adrenoceptor antagonists across the apical membrane of renal LLC-PK(1) cell monolayers. Br J Pharmacol 131, 71-79.

Gorboulev, V., Ulzheimer, J.C., Akhoundova, A., UlzheimerTeuber, I., Karbach, U., Quester, S., Baumann, C., Lang, F., Busch, A.E., and Koepsell, H. (1997). Cloning and characterization of two human polyspecific organic cation transporters. DNA Cell Biol 16, 871-881.

Grundemann, D., Hahne, C., Berkels, R., and Schomig, E. (2003). Agmatine is efficiently transported by non-neuronal monoamine transporters extraneuronal monoamine transporter (EMT) and organic cation transporter 2 (OCT2). J Pharmacol Exp Ther 304, 810-817.

Kimura, H., Takeda, M., Narikawa, S., Enomoto, A., Ichida, K., and Endou, H. (2002). Human organic anion transporters and human organic cation transporters mediate renal transport of prostaglandins. J Pharmacol Exp Ther 301, 293-298.

Urakami, Y., Akazawa, M., Saito, H., Okuda, M., and Inui, K. (2002). cDNA cloning, functional characterization, and tissue distribution of an alternatively spliced variant of organic cation transporter hOCT2 predominantly expressed in the human kidney. J Am Soc Nephrol 13, 1703-1710.